Colloids and Surfaces A 607 (2020) 125424

Contents lists available at ScienceDirect

Colloids and Surfaces A

journal homepage: www.elsevier.com/locate/colsurfa

Rapid sensing response for phenol with CuO nanoparticles

Rizwan Wahab[a,b,*], Farheen Khan[c], Naushad Ahmad[d], Manawwer Alam[d], Javed Ahmad[a,b], Abdulaziz A. Al-Khedhairy[a]

[a] Zoology Department, College of Science, King Saud University, Riyadh 11451, Saudi Arabia
[b] Chair for DNA Research, Zoology Department, College of Science, King Saud University, Riyadh 11451, Saudi Arabia
[c] Chemistry Department, Faculty of Science, Taibah University, Madina (Yanbu), Saudi Arabia
[d] Department of Chemistry, College of Science, King Saud University, Riyadh 11451, Saudi Arabia

GRAPHICAL ABSTRACT

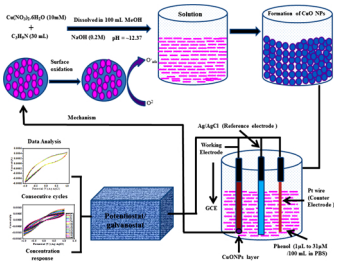

ARTICLE INFO

Keywords:
Copper oxide nanoparticles
Chronoamperometry
Electrochemical Sensor
Glassy carbon electrode
Modified electrode
Phenol

ABSTRACT

The human beings are directly or indirectly affected with the environmental pollution, excreted from the industries in the form of liquids such as inorganic and organic hazardous material. As compared to the inorganic chemicals, the organic aromatic compounds are more toxic for the nature. The phenol (PhOH), which is one the largest applied organic compounds in industries and hose hold chemical, which affect to the human health. Due to the wide applicability of copper oxide (CuO) nanomaterial in numerous areas such as optoelectronics, photocatalysis, solar cells, and energy evolution etc; easy to process and provide enhanced and rapid detectible responses against phenol is utilized in this study. The CuO-NPs were synthesized at low refluxing (at 65°C, 90 min) temperature and were well characterize via XRD (X-ray diffraction pattern), FESEM (Field emission scanning electron microscopy), TEM (Transmission electron microscopy) and FTIR (Fourier transform infrared spectroscopy), revels the spherical shaped morphology (~10 nm). The NPs were pasted on a glassy carbon electrode (GCE) to ascertain their sensing efficiency against PhOH via three electrode system. The efficiency of modified electrode was evaluated under different parameters,concentration effect of PhOH (very low, mid and high) (1, 10 and 31 μL/100 mL of PBS) tested and discloses that the sensor efficiency is very high and concentration dependent at all detectable limits. The formed sensor was also tested with different potentials from 1, 5, 10, 20, 50 and 100 mV/s and it's sequential to the potential. The chronoamperometry (CuO-NPs/GCE) was investigated in absence and presence and of PhOH at four different voltages +0.05 to +1.2 V from 0 to 1500*s* to observe the effect of time, which is time reliant. The reproducibility and stability were also tested in terms of cyclic response for seven days (RSD 2.13%), which further displayed that the processed sensor is much reliable for a longer period. To understand well, furthermore, a possible mechanism was also presented, based on obtained results.

* Corresponding author at: Zoology Department, College of Science, P.O. Box 2455, King Saud University, Riyadh 11451, Saudi Arabia.
E-mail address: rwahab@ksu.edu.sa (R. Wahab).

https://doi.org/10.1016/j.colsurfa.2020.125424
Received 17 May 2020; Received in revised form 26 July 2020; Accepted 12 August 2020
Available online 19 August 2020

1. Introduction

The environment is affected with various daily house hold hazardous materials and these hazardous material releases from industries and other sources. These harmful industrial effluents are directly or indirectly affected to the human beings in the form of organic, inorganic and other compounds. In a series of hazardous chemicals, the Phenol (PhOH), which is an aromatic compound and are extensively utilized in various industries for producing numerous products such as rubber, fertilizer, paint, drugs, petroleum and also uses in agricultural industry [1–2]. Although the PhOH is largely utilized as an industrial chemical for various purposes but at the same time it deliver several adverse effect on body and known as carcinogen, with a lethal dose ranging from 50-500 mg/kg in human beings, if swallowed orally [3]. Serious complaint were causes once exposes from PhOH and have an effect on human organs such as the heart, blood vessels, lungs, and kidneys, which may lead to convulsions, dizziness, irregular respiration, headache, nausea, drowsiness, cyanosis and others [1–3]. PhOH also affects the skin on contact causing pain, boils, and burns. Inhalation can cause pulmonary irritation and edema [1–3]. Water contaminated with PhOH can lead to serious problem's such as diarrhea, mouth sores, and darkening of urine. Similar toxicity also occurs in animals when exposed to PhOH [1–3]. Including this, other phenol derivatives (such as o-cresol, m-cresol, and p-cresol) are also noted atmospheric pollutants; however, PhOH is better known as a water pollutant [4]. PhOH often contaminates soil and drinking water due to exposure to industrial waste and it's also found in an essential organic compounds that largely used by the food industry for the production of fruit juices, beer, and wines, among others [5–6]. To this continuation, the removal of total inorganic continents from the water through microalgae cultivation was achieved to their high extends with co-flocculating process [7]. In this connection, the metal oxide and composite (Ni^{2+}-TiO_2/$CoFe_2O_4$) materials were utilized to degradate the organic dyes [8]. The results reveal that doping of Ni to composite TiO_2/$CoFe_2O_4$ and their calcined temperature; actively take part in photocatalytic degradation activities [8]. The PhOH is also used as a compound in various pharmaceuticals, pesticides, and dyestuffs [9], and is released as industrial effluent, contributing environmental degradation. Furthermore, it also affects the marine and fresh-water systems [10]. The Environmental Protection Agency (EPA, USA) has cited PhOH as a priority pollutant because of its persistence and high toxicity [11]. It's therefore, very important that PhOH continues to a topic of research in order to find a means of remediation, also known as a pesticide and fungicide [12]. As the production and utilization of PhOH involves various qualitative and quantitative controls, numerous means of regulating phenolic compounds have been developed [13–14]. However, more reliable methods are required for the detection of PhOH in liquid solutions with adequate sensitivity, so that substance can be detected and treated more efficiently [14–15]. Various investigative procedures such as mass spectrometry [16], HPLC [17], spectrophotometry [18], flow injection analysis (FI A) [19], and electrochemical methods [20–25] have all been used to discern PhOH concentrations in liquid samples [20–25]. The electrochemical techniques are cost-effective and easy-to-handle compared to other methods,which tend to be expensive and difficult to apply [21–22]. Due to their large surface areas and conductive and physicochemical characteristics, processed electrodes have been widely used for the electrochemical assessment in recent years [26]. A wide range of oxides and nanostructures is available for use in this field; CuO, which is a p-type semiconductor material [27], is available in the form of cuprous (BG = 2.17 eV) and cupric oxide (BG = 1.2-1.5 eV). Several methods have been used for the preparation of CuO nanoparticles (CuO-NPs), such as CVD (chemical vapor deposition) [28] and PECVD (plasma enhanced chemical vapor deposition) [29–30], etc. Chemical methods such as hydrothermal synthesis [31], spray pyrolysis [32], and solution combustion method [33] have also been utilized to develop the CuO nanostructures. These approaches generally require extensive care and need to use sophisticated instruments, and it's therefore, difficult to produce the structures in a large quantities without acquiring massive expense [34]. However, it is possible to produce nanostructures in bulk and at low cost through chemical solution process [35]. The synthesis of CuO-NPs from copper nitrate ($Cu(NO_3)_2.6H_2O$), propyl amine (C_3H_9N), and sodium hydroxide (NaOH) is investigated in this study, using the solution process at low temperatures (~65 °C) over a short reflux period (90 min). The detailed structure of the produced powder was investigated using FESEM and TEM, and the crystallinity, phase, and size of the particles were investigated with XRD. The synthesized material was used as a sensing material and a working electrode in order to check their efficiency in detecting PhOH in a PBS solution. FTIR was utilized to determine the functional characteristics of the prepared material. The potential of the processed copper oxide nanoparticles-based on GCE (CuO-NPs/GCE) was then measured to determine the oxidation and reduction that had occurred, using CV with different concentrations of PhOH.

2. Experimental

2.1. Chemicals

For the synthesis of copper oxide nanoparticles (CuO-NPs) chemicals such as copper nitrate hexahydrate, sodium hydroxide were received from the Aldrich chemical corporation Co. U.S.A and used without any further purification/modification.

2.2. Synthesis of the copper oxide nanoparticles (CuO-NPs)

The production of copper oxide nanoparticles (CuO-NPs) was carried out via solution synthesis using copper nitrate hexahydrate as the precursor material with the addition of n-propyl amine, and sodium hydroxide. In a typical experiment copper nitrate hexahydrate (10 mM), 30 mL of n-propyl amine and sodium hydroxide (0.2 M) were mixed with 100 mL of methanol (MeOH) under uniform stirring, producing a blue color solution. NaOH was then added slowly to this solution in a beaker and shaken. A pH of 12.37 was measured using a pH meter (Cole-Parmer, USA). The solution was then transferred into a refluxing pot and heated at 65 °C for 90 min. The solution was observed to change from blue to brown, and finally black as the refluxing temperature increased. The stable reaction product was then kept in the refluxing pot overnight at room temperature to cool. The cooled product was then transferred to a beaker and washed several times with solvent (alcohol, acetone, etc.) in order to eliminate any scum produced during the reaction. The formed material was then desiccated at room temperature and retained for analysis of the structural and chemical properties.

2.3. Materials Characterizations

The XRD (Rigaku, Japan) was utilized to determine the particle size, phase, and crystalline properties of the processed powder sample between 25º and 70º using $Cu_{K\alpha}$ radiation (λ = 1.54178 Å) at a scanning speed of 6º/min with an accelerating voltage of 40 kV and a current of 30 mA. The morphology of the prepared powder was examined using FESEM (Hitachi, Japan) at room temperature. To analyze the results from FESEM, the recovered powder was sprayed homogeneously onto a sample holder covered with carbon tape, which was subsequently coated with a conducting pt layer of 3*s*. In order to confirm the results, the powder was further investigated using TEM (JEOL JEM-2010 at 200 kV). The functional characteristics of the materials were also investigated with FTIR (Perkin Elmer-FTIR Spectrum-100, USA) analysis from 400-4000 cm^{-1} using KBr pellets.

2.4. Electrode modification

The NPs were used as an electron mediator/working electrode in order to determine the amount of PhOH present in the PBS buffer. The electrode was fabricated using CuO-NPs that were coated as film onto a GCE electrode (active surface area = 7×10^{-2} cm^2). The coating was constructed using a small number of NPs mixed with butyl carbitol acetate (BCA, at a ratio of 80:20), and the prepared slurry was coated onto the GCE electrode and dried at 60 ± 5 °C for 30-45 min in order to obtain a uniform layer over the entire surface of the electrode.

2.5. Electrochemical studies

The electrochemical analysis of the formed electrode was carried out using an autolab potentiostat/ galvanostat with the PGSTAT 204-FR A32 and NOVA software (Metrohom Autolab B.V. Kanaalweg 29-G, 3526 KM Utrecht, Netherlands) in a three electrode system [36–37]. The CuO-NPs/GCE electrode was used as the working electrode, a platinum (pt) wire was used as a counter electrode, and Ag/AgCl (sat.KCl) was utilized as reference electrode. The PBS solution (0.1 M; pH 7.2) containing the PhOH was used as the electrolyte solution for all electrochemical measurements. In order to investigate the concentration of PhOH with the CuO-NPs/GCE electrode, a range of different PhOH concentrations (1 µL to 31 µL/100 mL) were added to the PBS and a current between − 0.15 and +1.5 V were used to determine the sensing characteristics. The sensitivity and amperometric response with current-time (i-t) curves were measured in a 6 µM PBS solution.

2.6. Interference study of ions

The Interference study was conducted with using various metal salts and prepared the solution in a demineralized double distilled water (DMDW) at room temperature. The interference test was performed with three electrode system in presence of CuO-NPs/ GCE. Various ions (Na^+, Ag^+, Cd^{2+}, Pb^{2+}, Mn^{2+}, Co^{2+}, Zn^{2+}, Al^{3+}, Ni^{2+}, Fe^{3+}, CO_3^{2-}, CH_3COO^-, Cl^-, SO_4^{2-}) were added individually into the sample solution (150 µg/L) including tap and pond water sample under an optimized conditions.

3. Results and discussion

The size, phases, and crystallinity of the processed powder were evaluated using the same parameters as those described in section 2.3. The XRD spectra depicts peaks at defined positions such as 35.51°, 38.73°, 48.08°, 53.76°, 66.73°, and 75.17° are related to the crystal planes (Ī11), (111), (202), (020), (311), and (222) respectively. The XRD pattern shows peaks that are very similar to those produced by single crystalline CuO with no impurities, and matches with the standard JCPDS data card numbered 05-661 with crystal lattice constants at $a = 4.79$ Å, $b = 3.45$ Å, and $c = 5.32$ Å with a monoclinic structure.The pattern of XRD spectrum can be related to the formation of CuO nanoparticles (Fig. 1) [35], with no peaks other than those suggesting the presence of CuO, further confirms that the produced CuO is pure and free from any synthetic chemical impurities (Fig. 1) [35]. The average particle size of the prepared powder was calculated using the Scherrer equation [38]:

$$D = 0.9\ \lambda/\beta\ \cos\theta$$

Where λ is the wavelength of the X-ray radiation source, β is the full-width at half-maximum [FWHM] in radians, and θ is the Bragg diffraction angle and D represent the diameter of the particle. The diameters of the particles were thus calculated at approximately 10 nm.

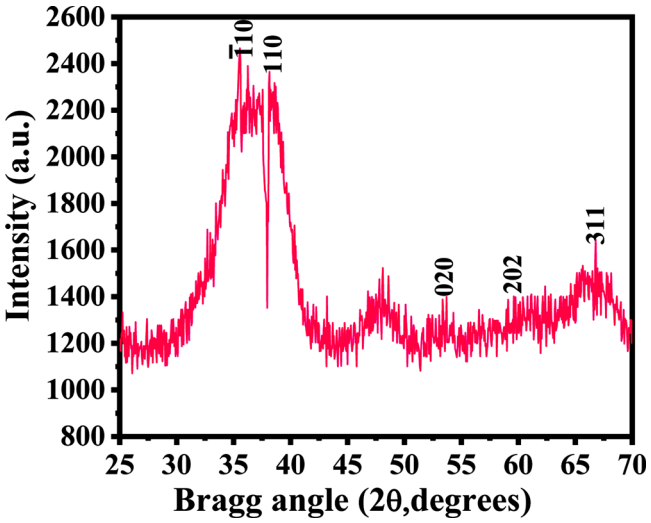

Fig. 1. X-ray diffraction pattern of the prepared copper oxide powder.

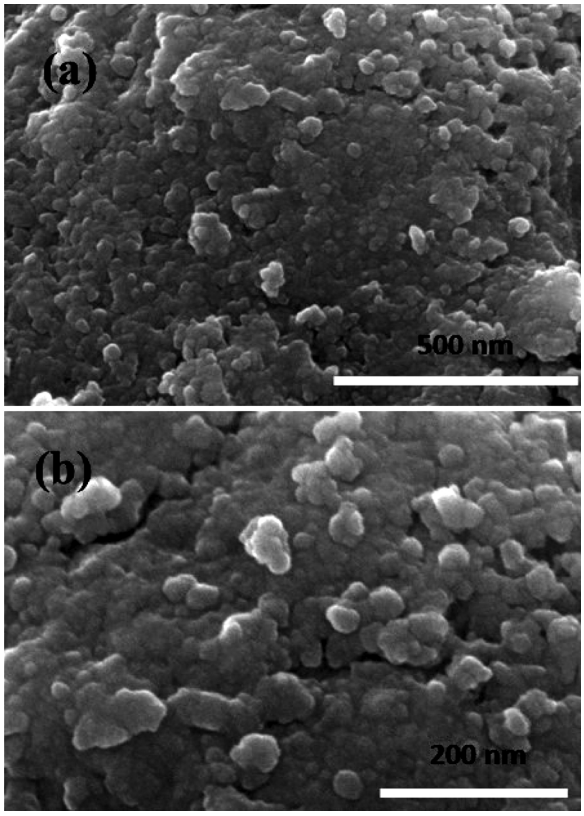

Fig. 2. FESEM images of CuO nanopowder: (a) apprehended at low magnification and (b) captured at high magnified scale.

3.1. Morphological Assessment (FESEM and TEM results)

The FESEM was used to assess the morphology of the grown powder, with the results given in Fig. 2. The obtained image (Fig. 2(a)), reveals that the NPs cover the whole surface of the sample holder and when close to scrutinization with a larger scale (Fig. 2(a)) confirms that the large numbers of nanoscale particles have been produced. The obtained particles are smooth, clean, and spherical (Fig. 2(a)) with an average size of ~10 nm. Fig. 2(b) is similar, indicating that the particles are spherical and heavily aggregated.

In order to understand more about the morphology of the processed material, the powder was further analyzed with TEM using the

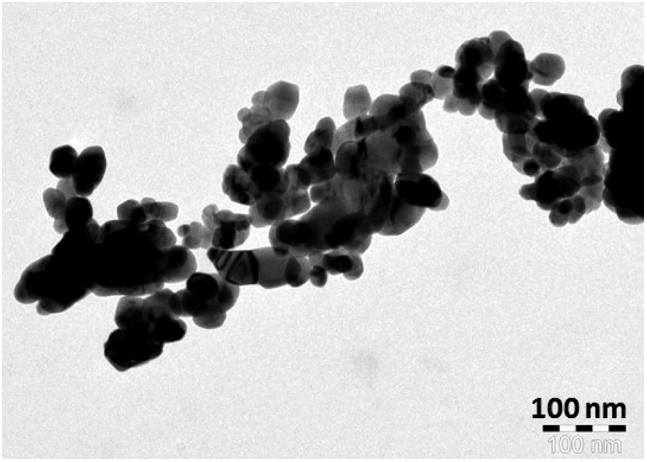

Fig. 3. TEM image of prepared CuO nanopowder.

parameters as defined in Section 2.3. The TEM observation revealed that the NPs are closely congregated, are of very small size, and have smooth surfaces. From the TEM image (Fig. 3), it is apparent that the width of each NP is ~10 nm and that the particles are consistently spherical in shape, confirming the results of the FESEM observation (Fig. 2a & b) [35,39–40].

3.2. FTIR Spectroscopy

The functional or chemical characteristic of the prepared material was analyzed using FTIR spectroscopy and the obtained spectrum is presented as Fig. 4. A very small amount of the processed powder was mixed with KBr and the amount of powder must be strictly controlled in order to produce good spectra. The FTIR spectrum indicates the presence of the copper nitrate and sodium hydroxide (NaOH) that were used in the production of the CuO-NPs. The broad peak between 3200 and 3600 cm^{-1} corresponds to the O-H (3443 cm^{-1}) stretching mode of water molecule, whereas the asymmetric stretching of the water molecules is centered at 1637 cm^{-1}. The small and sharp peak that is centered at 1430 cm^{-1} is associated with the stretching mode of NO_3^{2-} molecule [35,41–42]. A pointed sharp and long peak observed at approximately 540 cm^{-1} in the FTIR spectrum represents the CuO-NP formation. The functional information obtained from the FTIR confirms

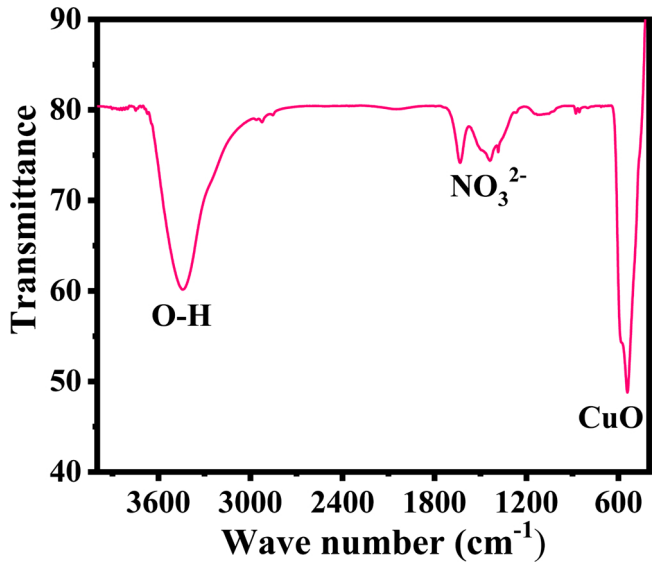

Fig. 4. FTIR spectrum which shows the functional characteristic of grown CuO nano powder.

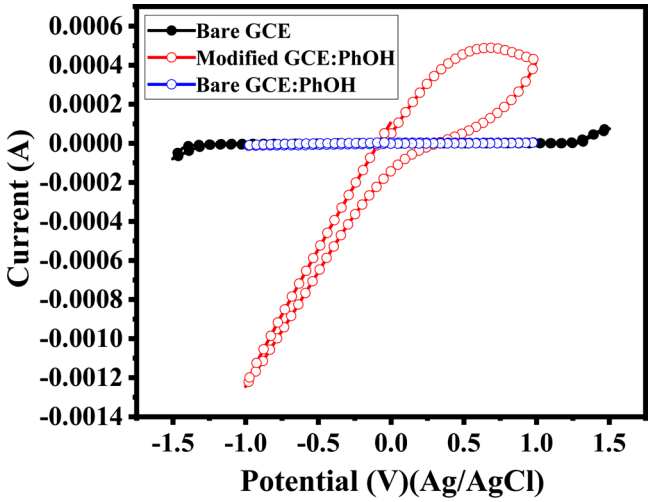

Fig. 5. Cyclic voltammograms of bare and modified electrodes in absence and presence of PhOH (6 μM) in 0.1 M PBS (pH 7.2). Scan rate: 100 mVs^{-1}.

the chemical properties of the prepared NPs, which is consistent with the data produced by the X-ray diffraction (Fig. 1).

3.3. Electrochemical/cyclic voltammetry (CV) studies

The fabricated electrode was initially tested without the CuO coating. No peak was detected in the obtained spectrum, from which it's clear that no oxidation/reduction occurred, and signifies that no potential was present on the bare electrode. The GCE was then coated with the CuO-NPs (over an area of 7×10^{-2} cm^2), and the electrochemical characteristics of the modified electrode was evaluated using CV to investigate PhOH (10 μL) in a 100 mL PBS (0.1 M, pH 7.2) solution (at a scan rate of 100 mV/s). The nanomaterial coated electrode (CuO-NPs/GCE) was further examined in presence of PhOH at two different concentrations (4 μM and 6 μM), on which phenol oxidation was clearly observed [43]. The potential and current (0.99 V, 4.27×10^{-4}, respectively) observed in the PhOH solution [43] confirms that the prepared electrode modified with CuO-NPs/GCE is much more efficient for both the transport of electrons and oxidization of the PhOH [44] solution (Fig. 5).

3.4. Effect of PhOH concentration on the modified electrode (CuO-NPs/GCE)

The current and potential (I-V curve) of CuO-NPs/GCE with concentrations of PhOH ranging from 1 μL to 31 μL in 100 mL PBS is presented in Fig. 6. The obtained spectrum shows a sequential change in the oxidation and reduction peaks from the lowest to the highest PhOH concentration, examined at 100 mV with a current potential range from −1.0 to 1.5 V. As can be seen in Fig. 6, the current at the anodic peak is directly correlated with the concentration of PhOH, rising as the PhOH concentration increases. Fig. 6 also suggests that the current resulting from the movement of ions increases with the increase in PhOH concentration, resembling the rapid transfer of electrons at the conduction band. A high potential was also observed at the anodic peak, in a previous experiment when PhOH was used at high levels of concentration (Fig. 6).

3.5. Effect of potential on the CuO-NPs/GCE electrode

In order to gain further details regarding the reliability of the modified CuO-NPs/GCE electrode, a series of different (1 to 100 mV/s) potentials were selected to further investigate the measurement carried out using the PBS solution, the result of which is presented in Fig. 7. A

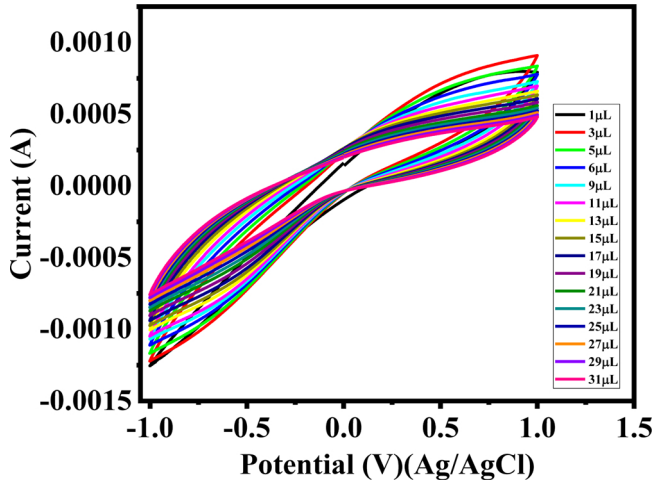

Fig. 6. Cyclic voltammetric responses of modified electrode as a function of PhOH concentration with scan rate of 100 mVs^{-1}.

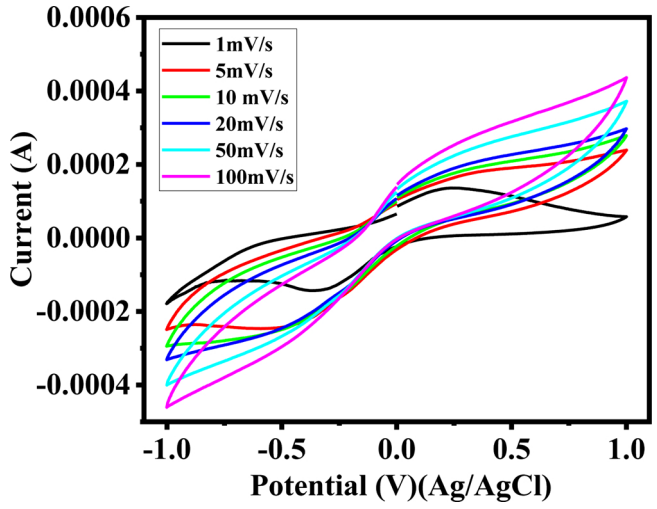

Fig. 7. Cyclic voltammetric responses of modified electrode in the presence of PhOH (6 µM) as a function of at different scan rates.

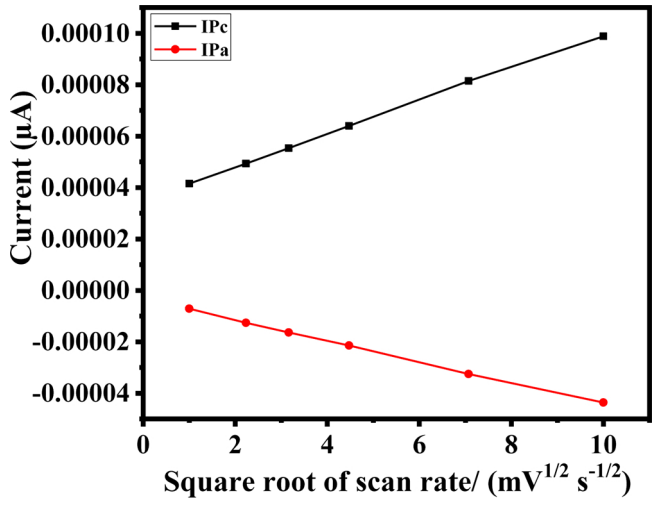

Fig. 8. Linear calibration graph for cathode and anode potentials of CuO-NPs/GCE.

Table 1
Detail calculation results for the LOD and LOQ.

S.No	Metal Oxide	LOD (µM)	LOQ (µM)	Correlation coefficient (R^2)
1.	CuO (IPa)	0.036	0.110	0.999
2.	CuO (IPc)	0.205	0.621	0.999

successive response was observed over different cycles using a fixed concentration of PhOH in 0.1 M PBS solution at a pH of 7.2. The graph obtained shows the relationship between the current and the enhancement in the potential of the fabricated PhOH sensor. At (1 mV/s) small anodic and cathodic peaks were observed in the spectrum, denoting a low potential; however, as the potential was increased, changes to the anodic and cathodic peaks were clearly seen in the spectrum, the CuO-NPs/GCE can be more sensitive for PhOH detection by increasing the voltage applied. Over the nanoparticles, the reduced graphene sheets in combination with Polypyrrole (PPy) (rGO @PPy) based electrode have similar information with the current experiment of electrochemical analysis and showed superior conductivity [45]. Based on the obtained data's, the linear plots were also constructed for the ionization potential of cathode (IPc) and ionization potential of anode (IPa) for the evaluation of correlation coefficient (R^2). It's observed in both (IPa & IPc) for CuO-NPs/GCE, the value of R^2 was 0.999 (Fig. 8). In addition to this, the limit of detection (LOD) for CuO-NPs/GCE (IPa) and CuO-NPs/GCE (IPc) were evaluated which were 0.036 and 0.205 respectively. The limit of quantitation (LOQ) for CuO-NPs/GCE (IPa) and CuO-NPs/GCE (IPc) were evaluated which were 0.110 and 0.621 respectively (Table 1) [46–47].

3.6. Chronoamperometry with the CuO-NPs/GCE electrode with and without PhOH

The chronoamperometry is an electrochemical technique in which the potential of the working electrode is periodical rather than continuous, and the resulting current from the faradaic processes occurs at the electrode and can be monitored as a function of time. The graph shows (Fig. 9) the steps that occur in the potential at set voltages, which are held constant over a specific period of time. The incremental response of the potential was measured over time from 0 to 100*s* in order to carry out a detailed observation of the selectivity and reproducibility of the prepared modified sensor (Fig. 9). The progressive response of the CuO-NPs/GCE based PhOH sensor was therefore, investigated using incremental time periods. The chronoamperometric curves of modified

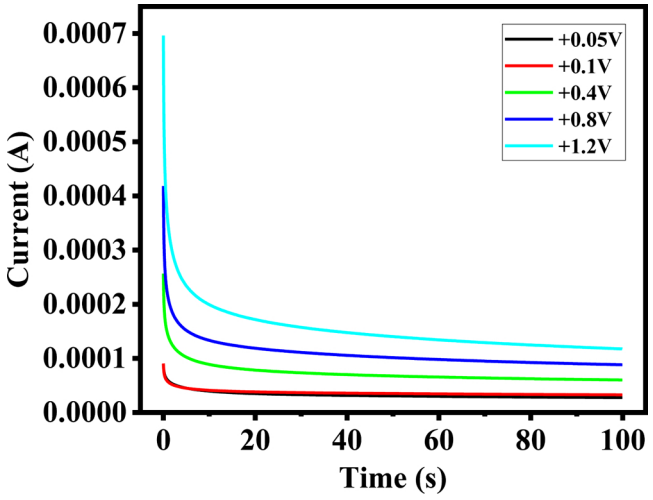

Fig. 9. Chronoamperometric (A/s) curves of modified electrode in absence (a) and presence (b) of PhOH (6 µM) as a function of at different applied potentials in 0.1 M PBS (pH 7.2).

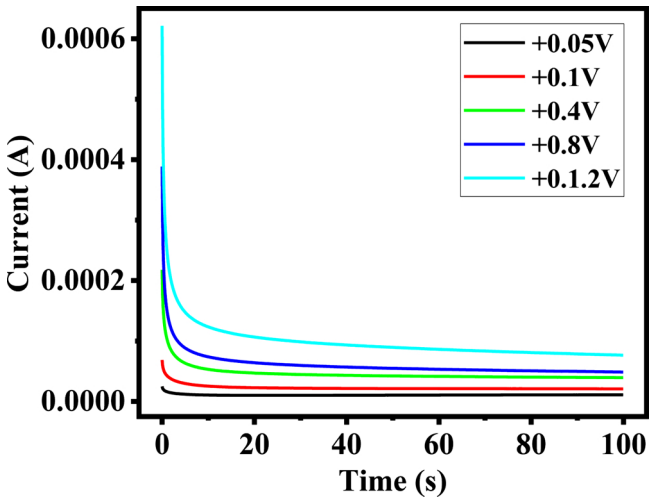

Fig. 10. Chronoamperometric current–time (A/s) response of modified electrode with successive addition of different concentrations of PhOH to in 0.1 M PBS (pH 7.2) at an applied potential of + 0.8 V (vs. Ag/AgCl).

Table 2
The chronoamperometry responses with the modified CuO-NPs/GCE electrode in absence and presence of PhOH

Operating voltage	Response time in seconds (*s*)	Chronoamperometry responses in absence of PhOH (A/s)	Chronoamperometry responses in presence of PhOH (A/s)
+0.05 V	0	8.89×10^{-5}	2.48×10^{-5}
	20	3.84×10^{-5}	1.00×10^{-5}
	40	3.15×10^{-5}	1.02×10^{-5}
	60	2.98×10^{-5}	1.06×10^{-5}
	80	2.85×10^{-5}	1.08×10^{-5}
	100	2.74×10^{-5}	1.11×10^{-5}
+0.10 V	0	9.04×10^{-5}	6.86×10^{-5}
	20	3.80×10^{-5}	2.27×10^{-5}
	40	3.57×10^{-5}	2.16×10^{-5}
	60	3.43×10^{-5}	2.13×10^{-5}
	80	3.33×10^{-5}	2.10×10^{-5}
	100	3.25×10^{-5}	2.08×10^{-5}
+0.40 V	0	2.56×10^{-4}	2.17×10^{-4}
	20	7.83×10^{-5}	4.69×10^{-5}
	40	6.99×10^{-5}	4.32×10^{-5}
	60	6.54×10^{-5}	4.15×10^{-5}
	80	6.23×10^{-5}	4.03×10^{-5}
	100	6.00×10^{-5}	3.94×10^{-5}
+0.80 V	0	4.18×10^{-4}	3.88×10^{-4}
	20	1.18×10^{-4}	6.40×10^{-5}
	40	1.05×10^{-5}	5.68×10^{-5}
	60	9.78×10^{-5}	5.32×10^{-5}
	80	9.23×10^{-5}	5.07×10^{-5}
	100	8.81×10^{-5}	4.87×10^{-5}
+1.20 V	0	6.96×10^{-4}	6.21×10^{-4}
	20	1.71×10^{-4}	1.06×10^{-4}
	40	1.47×10^{-4}	9.34×10^{-5}
	60	1.34×10^{-4}	8.61×10^{-5}
	80	1.24×10^{-4}	8.08×10^{-5}
	100	1.17×10^{-4}	7.65×10^{-5}

electrode (CuO-NPs/GCE) were first produced in absence of PhOH at different voltages (+0.05 to +1.2 V). The chronoamperometry was also carried out using the CuO-NPs/GCE in presence of PhOH at specific voltage ranges (+0.05 to 1.2 V) between 0 and 100*s*, with changes observed in the current over time (Fig. 10). At 0*s* and +0.05 V a very low current was observed (2.48×10^{-5}), which increased at 20, 40, 60, 80, and 100*s* to 1.00×10^{-5}, 1.02×10^{-5}, 1.06×10^{-5}, 1.08×10^{-5}, and 1.11×10^{-5}, respectively [48–49]. From most of the results it's concluded that the current is increases in presence of PhOH, which

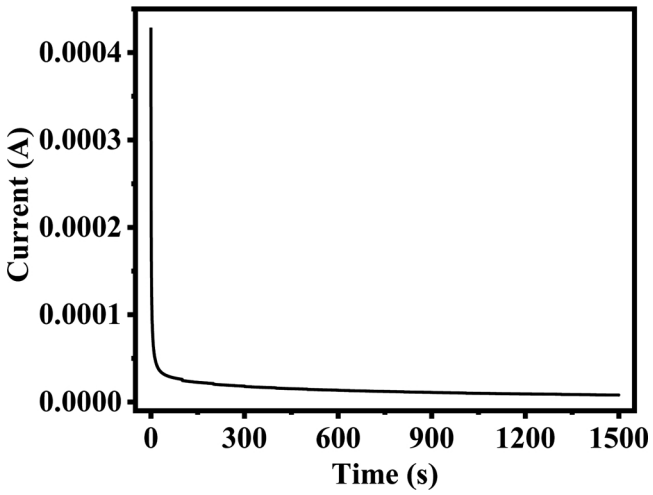

Fig. 11. Amperometric response of CuO-NPs/GCE with successive addition of phenol into 0.1 M PBS (pH 7.2), which depicts the time (0 to 1500 *s*) and current spectra for the reliability and reproducibility of the optimized data.

further shows the response of modified CuO-NPs/GCE electrode (Table 2).

3.7. Effect of time response of CuO-NPs/GCE electrode with PhOH

The effect of time on the modified electrode CuO-NPs/GCE was also observed over the period from 0 to 1500*s*, using PhOH for the evaluation of the sensor selectivity and reproducibility (Fig. 11). A systematic change was observed at different times for the prepared CuO-NPs/GCE based PhOH sensor. At 0 *s* the response to the current was (4.28×10^{-4}) and at 100, 200, 300, 400, 500, 600, 700, 800, 900, 1000, 1100, 1200, 1300, 1400 and 1500*s*, the currents were observed to 2.59×10^{-5}, 2.04×10^{-5}, 1.82×10^{-5}, 1.63×10^{-5}, 1.47×10^{-5}, 1.35×10^{-5}, 1.264×10^{-5}, $1.1\,8 \times 10^{-5}$, 1.11×10^{-5}, 1.04×10^{-5}, 9.79×10^{-6}, 9.26×10^{-6}, 8.93×10^{-6}, 8.46×10^{-6} and 8.02×10^{-6} respectively. The obtained sequential and systematic data reveals that the present sensor is specific, selective, and reproducible, exhibiting sustainability and reliability over extended periods of time [37].

3.8. Consecutive cyclic response of the modified electrode (CuO-NPs/GCE)

The reproducibility and stability of the CuO-NPs/GCE sensor was

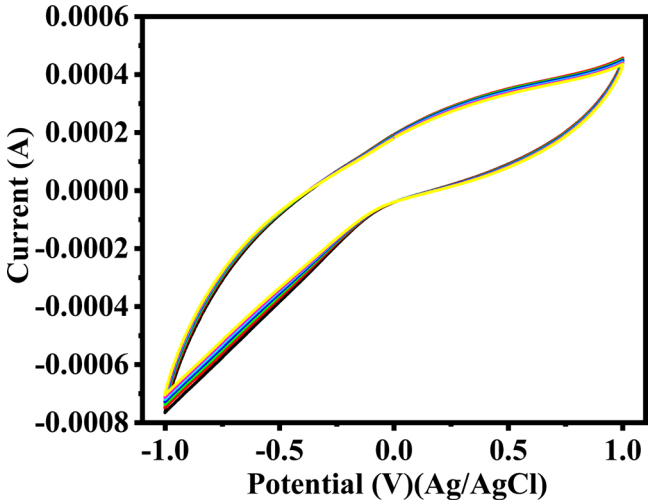

Fig. 12. Seven consecutive cycles for the sample in presence of 6 μM (PhOH) in 0.1 M PBS at scan rate of 100 mV/s.

also tested using a cyclic test investigating the responses of electrode and the obtained data is presented as Fig. 12. The graph shows seven consecutive cycles of the CuO-NPs/GCE electrode in presence of 6 μM of PhOH in a 0.1 M PBS solution, demonstrating the excellent reproducibility over consecutive measurements. Tests were carried out between the first and the seventh day. The prepared sensor was kept in an ambient atmosphere over this period, during which a little change was observed in the shape of the voltammetric cycle, again confirming the long-term stability of the produced sensor. The experimental relative standard deviation (RSD) was found to be 2.13%, confirming the reproducibility of the prepared electrode. The results confirm that the CuO-NPs/GCE electrode exhibits high stability with good reproducibility, and that it is sustainable over long periods and is therefore applicable for practical uses [43].

3.9. Interference test

The interference test was also conducted with cyclic voltammetry with a series of metal ions (cations and anions). The metal salts solutions were prepared in DMDWand analyzed the interference with three electrode system in presence of CuO-NPs/GCE. Various metal ions (Na^+, Ag^+, Cd^{2+}, Pb^{2+}, Mn^{2+}, Co^{2+}, Zn^{2+}, Al^{3+}, Ni^{2+}, Fe^{3+}, CO_3^{2-}, CH_3COO^-, Cl^-, SO_4^{2-}) were added individually into sample solution (150 μg/L) under the optimized conditions. Especially, the cyclic voltammetry test was conducted with each metal ion and recorded from the range of +1.5 to -1.5 V at room temperature. Each interfering species had different redox potentials, the response current value was not much reflected, which were evidently distinguished. The peak current was not disturbed by concentration of interfering metal ions and the modified electrode was well responses as can be seen in Fig. 13. Therefore, the different metal ions did not interfere in the solutions and had not showed significant effect. The higher redox potential support CuO-NPs/GCE system in PBS than the other competing metal ions. Hence, CuO-NPs/GCE was used as a selective for material to determine CV with different metal ions concentrations. The stronger response of CuO-NPs shows more adhesion on the surface of electrode and overcome of weakened ions. Generally, the response of interfering metal ions in real samples such as tap and pond water did show interfere with in the detectable limits. The study of interfering metal ions gives surety concerned sensibility, selectivity and applicability of nanomaterials, which is the requirements of the environmental and hazardous sample study at quality standard [50–51].

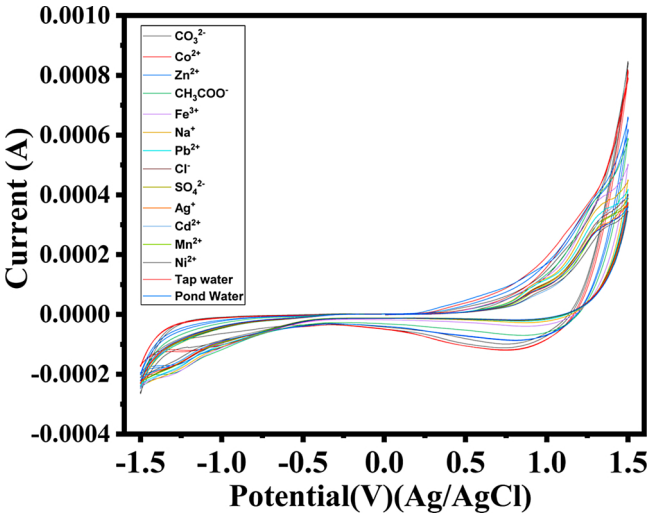

Fig. 13. Cyclic voltammetry responses for the interference metal ions in presence of CuO-NPs/GCE.

4. Possible mechanism and discussion

Copper oxide (CuO) is an interesting semiconductor material due to their unique physicochemical properties and a large band gap. The nanostructure of the material processed enhances the electrical conductivity. Based on the obtained results related to use of nanostructured material, utilized as a sensor material for the detection of PhOH in liquid medium. This is well documented that the PhOH is a highly toxic material and also it's largely used in an industry for the formation of various products. Due high toxicity rate of the chemical, therefore it's an urgent demand that the sensing of PhOH need to be cost effective and can be identified even at lower concentration in any liquid medium. In this experiment, we have opted to investigate a wide range of PhOH concentrations (1 μL to 31 μL/100 mL in PBS (0.1 M)) and tested the sensing efficiency of modified working electrode (CuO-NPs/GCE) to detect the PhOH via the electrochemical method. In this study, the CuO-NPs/GCE plays an important role in process of electron transport as evident from the CV data with bare and modified electrode (Fig. 5), also preliminary detection information of PhOH. A detailed concentration range (1 μL to 31 μL/100 mL in PBS (0.1 M)) was opted to know the CuO-NPs/GCE sensor steadiness. The obtained data shows that the semiconductor sensor material (CuO-NPs) is highly applicable and concentration dependent at every detectible limit for to detect the PhOH even at a very low concentration (Fig. 6). The different potential window also justifies that the chosen sensor material is much effective against PhOH and provide responses correspondingly (Fig. 7). The correlation coefficient (R^2 = 0.999) for the ionization potentials of cathode and anodes (IPc and IPa) were examined (Fig. 8) for the processed CuO-NPs/GCE sensor. The limit of detection (LOD) and quantitation (LOQ) were also evaluated (Table 1). The chronoamperometry responses for the absence and presence of PhOH with a fixed operating voltage (A/s) provides a detailed out line related to the obtained current from the faradaic processes, which occurs at the electrode (CuO-NPs/GCE) and can be monitored as a function of time. The increase in the potential with time from 0 to 100*s* shows a response in order to carry out detailed information related to selectivity and reproducibility of the prepared modified sensor. It assumes that due to the higher and longer period stability and reproducibility, the CuO-NPs/GCE electrode can be utilized for the large scale industrial and environmental samples detection of PhOH, as can be seen from the data concerning cyclic usage and reproducibility. The longer cyclic (seven days) response for the modified electrode (CuO-NPs/GCE), detection of PhOH justifies that the electrode (CuO-NPs/GCE) exhibit higher stability, sustainable and reproducible in nature. The basic principle for the developed modified CuO-NPs/GCE works on varying concentration of analyte (PhOH) and measured the adsorption and conductance of the analyte with CuO-NPs/GCE electrode. After the prepared CuO nanostructures were deposited as described in section 2.5 onto the GCE, once the electrode was completely formed, it was immersed in PBS with different concentrations of analyte (PhOH, 1 to 31 μL/100 mL). The surface of the modified CuO-NPs/GCE has the ability to trap and absorb atmospheric oxygen, and this atmospheric oxygen can spill over the whole surfaces of the electrode, which further ionized (O_{-ads}) via the removal of electrons at the conduction band and then oxidized (O- or O^{2-}) on the surface layer of the CuO-NPs/GCE. In second step, the electrolyte, which already have the negative charged oxygen molecule trapped and electrons are back to the conduction band on the surfaces of electrode. In this process, it forms a charged layer between the electrode (CuO-NPs/GCE) and the analyte molecule [45,48–49]. The obtained CV data for oxidation and reduction for a series of concentration, varied potential, time and cyclic responses for the reproducibility, sustainability support the sensing mechanism. The charged or oxidized oxygen was adsorbed onto the surface of the electrode has the capability to amplify the potential of the prepared electrode, and can improve the resistance of the processed assemblage. Such experiment leads to a reduction in the conductance and an increase in the potential of the (CuO-NPs/GEC)

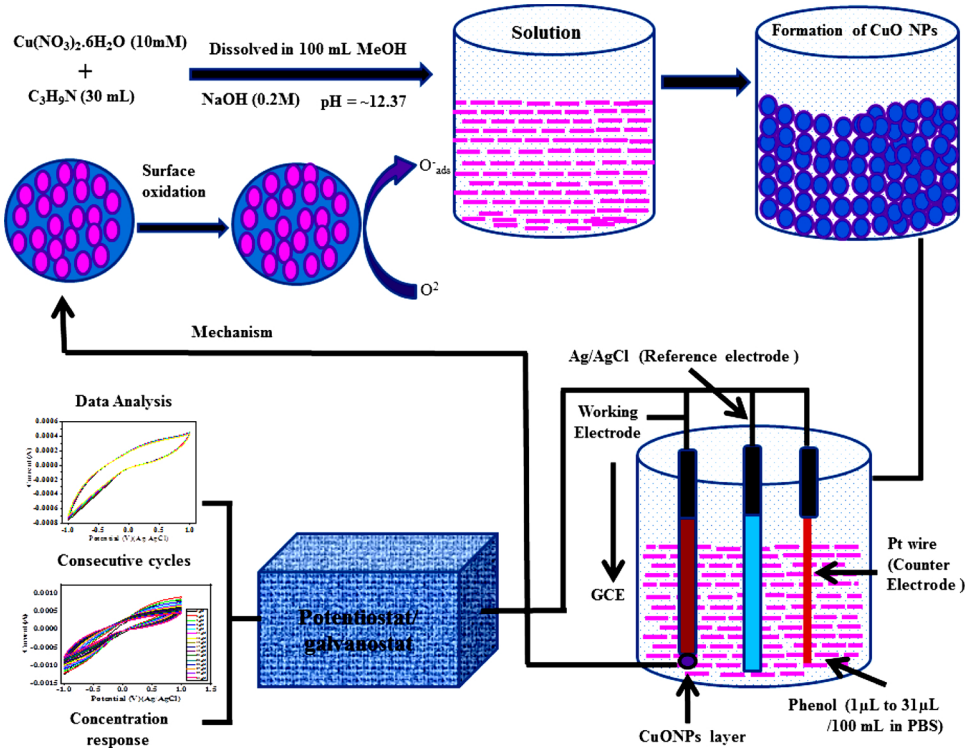

Fig. 14. Schematic illustration of experimental setup, sensing and analysis of acquired data.

electrode. In this study, it's hypothesized that changing the concentration (low to high) of the analyte (PhOH) leads to higher efficiency and greater resistivity. The result of sensor data much influenced by the nanostructure type with variation occurring in the results when different architectures were utilized such as rods, flowers, tubes, wires, or belts are used; or the pH, electrolytes, chemical properties, and processes for preparation of the electrode are used. The spherical shaped structure of the NPs is utilized in this experiment, which exhibit large surface areas and an increase in the band gap in which the electron transportation channels are generated, provides an enhanced capacity for sensing. The nanostructure of the semiconductors provides numerous passages for the analyte via adsorption. With increased sensitivity, the stability and enhanced reproducible properties of semiconductor materials leads to the significant transportation of electrons between the electrode film (CuO-NPs) and the analyte (PhOH) (as sketched Fig. 14). Additionally, the immobilization of the nanostructures on the surface of the electrode directly affects the reaction/response time and this can be easily visualized in the electrical signals that occur in the produced sensor. The process was significantly improved with the utilization of a suitable catalyst spread over the surface of the CuO-NPs/GEC electrode. In this case the PhOH acts as an analyte in the reaction and plays a prominent role in increasing the reaction with the available oxygen that is absorbed onto film/layer at the surface (CuO-NPs). This also enhanced the conductance and the response of CuO-NPs/GEC electrode [52–55].

5. Conclusions

The summary of the present work illustrates that the CuO-NPs were successfully synthesized through solution process. The characterizations revels that the obtained NPs are very small having ~10 nm in diameter, spherical in shape and clustered form with good chemical characteristic. The CuO-NPs were well applied as electrode material CuO-NPs/GCE against to hazardous PhOH. From the sensor detection study, it's obtained from the cyclic voltammetry (CV) that the modified sensor successfully works from a low to high range of PhOH (1 µL to 31 µL PhOH/100 mL) in PBS. The chronoamperometry data for modified electrode CuO-NPs/GCE in absence and presence of PhOH also justifies that at specified voltages such as +0.05, +0.10, +0.40 V, +0.80 V and +1.20 V with defined time intervals (0 to 100*s*) displayed the responses in term of signal change. From the observed chronoamperometry data, it depicts that the current rate enriched with presence of PhOH as compared to in absence of PhOH in the solution, this again shows that modified CuO-NPs/GCE is successfully work at low to high range of potential. The seven days scan cycle data also reveals that the modified sensor CuO-NPs/GCE is reliable, reproducible and sustainable for the longer periods. The interference test of various ions were also conducted against the CuO-NPs/GCE for to check of their sensitivity and selectivity, which reveals that no interference was observed at significant level that's mean the processed sensor, is highly responsive for the environmental samples. It may assume that the produced sensor will be suitable for various industrial purposes to check their toxicity rate from a low to high concentrations range of hazardous chemicals.

CRediT authorship contribution statement

Rizwan Wahab: Conceptualization, Methodology, Investigation, Resources, Data curation, Writing - original draft, Writing - review & editing, Supervision, Project administration, Funding acquisition. **Farheen Khan:** Methodology, Validation, Formal analysis, Data curation. **Naushad Ahmad:** Methodology, Software, Validation, Formal analysis, Data curation. **Manawwer Alam:** Methodology, Software, Validation, Formal analysis, Resources, Data curation. **Javed Ahmad:** Formal analysis, Data curation. **Abdulaziz A. Al-Khedhairy:** Methodology, Resources.

Declaration of Competing Interest

The authors declare that they have no known competing financial interests or personal relationships that could have appeared to influence the work reported in this paper.

Acknowledgements

The authors are grateful to the Deanship of Scientific Research, King Saud University for funding through Vice Deanship of Scientific Research Chairs.

References

[1] P. Saravanan, K. Pakshirajan, P. Saha, Treatment of phenolics containing synthetic wastewater in an internal loop airlift bioreactor (ILALR) using indige- nous mixed strain of Pseudomonas sp. under continuous mode operation, Bioresour. Technol 100 (2009) 4111–4116.
[2] R. Maallah, A. Moutcine, C. Laghlimi, M.A. Smaini, A. Chtaini, Electrochemical biosensor for degradation of phenol in the environment, Sensing and Bio-Sensing Research 24 (2019) 100279.
[3] IARC, Monographs on the Evaluation of the Carcinogenic Risk of Chemicals to Humans, World Health Organization, International Agency for Research on Cancer, Geneva, 1999 1972-PRESENT. http://monographs.iarc.fr/ENG/Classification/index.php p. V71 762.
[4] S.E. Manahan, Fundamental of Environmental Chemistry, Lewis, Boca Raton, 1993, p. 618 ISBN-13: 978-0873715874.
[5] A. Morales, D.A. Birkholz, S.E. Hrudey, Analysis of pulp mill effluent contamination in water, sediment and fish bile fatty and resin acids, Water Environ.Res 64 (1992) 660–668.
[6] G.K. Buckee, Determination of the volatile components of beer, J. Inst. Brew 98 (1992) 78–79.
[7] Y. Zhang, Z. Xiong, L. Yang, Z. Ren, P. Shao, H. Shi, X. Xiao, S.G. Pavlostathis, L. Fang, X. Luo, Successful isolation of a tolerant co-flocculating microalgae towa rds highly efficient nitrogen removal in harsh rare earth element tailings (REEs) wastewater, Water Res. 166 (2019) 115076.
[8] F. Deng, Y. Li, S. Peng, X. Luo, S. Luo, Photocatalytic Degradation of Methyl Orange by Ni^{2+}-Doped Anatase TiO_2/$CoFe_2O_4$ Composites Under Solar Light Irradiation, Asian Journal of Chem 23 (7) (2011) 2874–2878.
[9] R. Tyagi, Determination of substituted phenols in water by gas chromatography/mass spectroscopy after solid phase extraction, Fresenius Environ. Bull 4 (1995) 751–759.
[10] W. Duan, F. Meng, Y. Lin, G. Wang, Toxicological effects of phenol on four marine microalgae, Environ. Toxicol. Pharmacol 52 (2017) 170–176.
[11] W.W. Anku, M.A. Mamo, P.P. Govender, Phenolic Compounds in Water: Sources, Reactivity, Toxicity and Treatment Methods, Ch17, Intech open Publication.
[12] V.I. Lushchak, T.M. Matviishyn, V.V. Husak, J.M. Storey, K.B. Storey, Pesticide toxicity: A mechanistic approach, EXCLI J 17 (2018) 1101–1136 ISSN 1611- 2156.
[13] J. Michałowicz, W. Duda, Phenols – Sources and Toxicity, Polish J. of Environ. Stud. 16 (3) (2007) 347–362.
[14] P.M.V. Schie, L.Y. Young, Isolation and Characterization of Phenol-Degrading Denitrifying Bacteria, Appl. Environ. Microbio 64 (7) (1998) 2432–2438.
[15] C.D. Stalikas, Extraction, separation, and detection methods for phenolic acids and flavonoids, J. Sep. Sci. 30 (2007) 3268–3295.
[16] F.W. Karasek, S.H. Kim, H.H. Hill, Mass identified mobility spectra of p-nitro phenol and reactant ions in plasma chromatography, Anal. Chem. 48 (1976) 1133–1136.
[17] F. Elbarbry, K. Wilby, J. Alcorn, Validation of a HPLC method for the determina tion of p-nitro phenol hydroxylase activity in rat hepatic microsomes, J. Chroma- togr. A 834 (2006) 199–203.
[18] A. Niazi, A. Yazdanipour, Spectrophotometric simultaneous determination of nitrophenol isomers by orthogonal signal correction and partial least squares, J. Hazard Mater 146 (2007) 421–427.
[19] M. Miró, A. Cladera, J.M. Estela, V. Cerda, Dual wetting-film multi-syringe flow injection analysis extraction application to the simultaneous determination of nitro phenols, Anal. Chim. Acta. 438 (2001) 103–116.
[20] D.D. Souza, L.H. Mascaro, O.F. Filho, A Comparative Electrochemical Behaviour Study and Analytical Detection of the p-Nitrophenol Using Silver Solid Amalgam, Mercury, and Silver Electrodes, Int. J. Anal. Chem (2011) 726462.
[21] L. Chu, L. Han, X. Zhang, Electrochemical simultaneous determination of nitro phenol isomers at nano-gold modified glassy carbon electrode, J. Appl. Electrochem. 41 (2011) 687–694.
[22] P. Deng, Z. Xu, J. Li, Simultaneous voltammetric determination of 2-nitrophenol and 4-nitrophenol based on an acetylene black paste electrode modified with a graphene-chitosan composite, Microchim. Acta 181 (2014) 1077–1084.
[23] V.A. Pedrosa, L. Codognoto, A.S.M. Sergio, A. Avaca, Is the boron-doped diamond electrode a suitable substitute for mercury in pesticide analyses? A comparative study of 4-nitrophenol quantification in pure and natural waters, J. Electroanal. Chem. 573 (2004) 11–18.
[24] B. Yosypchuk, L. Novotny, Nontoxic electrodes of solid amalgams, Crit. Rev. Anal. Chem. 32 (2002) 141–151.
[25] Ø. Mikkelsen, K.H. Schrøder, Amalgam electrodes for electroanalysis, Electro analysis 15 (2003) 679–687.
[26] K.S. Khachatryan, S.V. Smirnova, I.I. Torocheshnikova, N.V. Shvedene, A.A. Formanovsky, I.V. Pletnev, Solvent extraction and extraction–voltammetric determination of phenols using room temperature ionic liquid, Anal. Bioanal. Chem 381 (2) (2005) 464–470.
[27] Y. Wang, S. Lany, J. Ghanbaja, Y. Fagot-Revurat, Y.P. Chen, F. Soldera, D. Horwat, F. Mucklich, J.F. Pierson, Electronic structures of Cu_2O, Cu_4O_3, and CuO: A joint experimental and theoretical study, Physical Rev. B 94 (2016) 245418.
[28] D. Barreca, E. Comini, A. Gasparotto, C. Maccato, C. Sada, G. Sberveglieri, E. Tondello, Chemical vapor deposition of copper oxide films and entangled quasi-1D nanoarchitectures as innovative gas sensors, Sensors and Actuators B 141 (2009) 270–275.
[29] Q. Simon, D. Barreca, A. Gasparotto, C. Maccato, E. Tondello, C. Sada, E. Comini, G. Sberveglieri, M. Banerjee, K. Xu, A. Devi, R.A. Fischer, CuO/ZnO Nanocomposite Gas Sensors Developed by a Plasma-Assisted Route, Chem Phys Chem 13 (9) (2012) 2342–2348.
[30] S. Eisermann, A. Kronenberger, A. Laufer, J. Bieber, G. Haas, S. Lautenschläger, G. Homm, P.J. Klar, B.K. Meyer, Copper oxide thin films by chemical vapor deposition: Synthesis, characterization and electrical properties, Physica Status solidi a 209 (3) (2012) 531–536.
[31] M. Outokesh, M. Hosseinpour, S.J. Ahmadi, T. Mousavand, S. Sadjadi, W. Soltanian, Hydrothermal Synthesis of CuO Nanoparticles: Study on Effects of Operational Conditions on Yield, Purity, and Size of the Nanoparticles, Ind. Eng. Chem. Res 50 (6) (2011) 3540–3554.
[32] V. Saravanan, P. Shankar, G.K. Mani, J.B.B. Rayappan, Growth and Characterization of spray pyrolysis deposited copper oxide thin films: Influence of substrate and annealing temperatures, J. Analytical and Applied Pyrolysis 111 (2015) 272–277.
[33] A. Ashok, A. Kumar, R.R. Bhosale, M.A.H. Saleha, L.J.P.V.D. Broeke, Cellulose assisted combustion synthesis of porous Cu–Ni nanopowders, RSC Adv 5 (2015) 28703–28712.
[34] A.S. Ethiraj, D.J. Kang, Synthesis and characterization of CuO nanowires by a simple wet chemical method, Nanoscale Res Lett 7 (2012) 70.
[35] R. Wahab, S.T. Khan, S. Dwivedi, M. Ahamed, J. Musarrat, A.A. Al-Khedhairy, Effective inhibition of bacterial respiration and growth by CuO microspheres composed of thin nanosheets, Colloids and Surfaces B: Biointerfaces 111 (2013) 211–217.
[36] F. Ahmed, S. Kumar, N. Arshi, M.S. Anwar, B.H. Koo, C.G. Lee, Rapid and cost effective synthesis of ZnO nanorods using microwave irradiation technique, Funct. Mater.Lett. 4 (1) (2011) 1–5.
[37] R. Wahab, N. Ahmad, M. Alam, A.A. Ansari, Nanocubic magnesium oxide: towards hydrazine sensing, Vacuum 155 (2018) 682–688.
[38] B.D. Cullity, Elements of X-ray Diffraction, Addison-Wesley Publishing Company, Reading, MA, 1978.
[39] L. Dörner, C. Cancellieri, B. Rheingans, M. Walter, R. Kägi, P. Schmutz, M.V. Kovalenko, L.P.H. Jeurgens, Cost-effective sol-gel synthesis of porous CuO nanoparticle aggregates with tunable specific surface area, Sci. Rep. 9 (2019) 11758.
[40] N. Silva, S. Ramírez, I. Díaz, A. Garcia, N. Hassan, Easy, Quick, and ReproducibleSonochemical Synthesis of CuO Nanoparticles, Materials 12 (2019) 804.
[41] S. Sonia, N.D. Jayram, P.S. Kumar, D. Mangalaraj, N. Ponpandian, C. Viswanathan, Effect of NaOH concentration on structural, surface and antibacterial activity of CuO nanorods synthesized by direct sonochemical method, Superlattices and Microstruc. 66 (2014) 1–9.
[42] S. Yu, J. Liu, W. Zhu, Z.T. Hu, T.T. Lim, X. Yan, Facile room-temperature synthesis of carboxylated graphene oxide-copper sulfide nanocomposite with high photodegradation and disinfection activities under solar light irradiation, Sci. Rep. 5 (2015) 16369.
[43] N. Ahmad, M. Alam, R. Wahab, J. Ahmad, M. Ubaidullah, A.A. Ansari, N.M. Alotaibi, Synthesis of NiO–CeO_2 nanocomposite for electrochemical sensing of perilous 4-nitrophenol, J. Mater. Sci.: Materials in Electronics 30 (2019) 17643–17653.
[44] D.M. Yerga, E.C. Rama, A.C. García, Electrochemical Study and Determination of Electroactive Species with Screen-Printed Electrodes, J. Chem. Educ. 93 (7) (2016) 1270–1276.
[45] L. Yang, G. Yi, Y. Hou, H. Cheng, X. Luo, S.G. Pavlostathis, S. Luo, A. Wang, Building electrode with three-dimensional macroporous interface from biocompatible polypyrrole and conductive graphene nanosheets to achieve highly efficient microbial electrocatalysis, Biosensors and Bioelectronics 141 (2019) 111444.
[46] International Organization for Standardization Accuracy (Trueness and Precision) of Measurement Methods and Results, (1994) ISO/DIS: 5725.
[47] R. Wahab, F. Khan, Y.K. Mishra, J. Musarrat, A.A. Al-Khedhairy, Antibacterial studies and statistical design set data of quasi zinc oxide nanostructures, RSC Adv. 6 (2016) 32328–32339.
[48] S.M. Pawar, J. Kim, A.I. Inamdar, H. Woo, Y. Jo, B.S. Pawar, S. Cho, H. Kim, H. Im, Multi-functional reactively-sputtered copper oxide electrodes for supercapacitor and electro-catalyst in direct methanol fuel cell applications, Sci. Rep. 6 (2016) 21310.
[49] A.T.G. Esparza, K. Limkrailassiri, F. Leroy, S. Rasul, W. Yu, L. Lin, K. Takanabe, Photoelectrochemical and electrocatalytic properties of thermally oxidized copper oxide for efficient solar fuel production, J. Mater. Chem. A 2 (2014) 7389–7401.
[50] N.M. Thanh, N.D. Luyen, T.T.T. Toan, N.H. Phong, N.V. Hop, Voltammetry Determination of Pb(II), Cd(II), and Zn(II) at Bismuth Film Electrode Combined with 8-Hydroxyquinoline as a Complexing Agent, Journal of Analytical Methods in Chemistry (2019) 11. Article ID 4593135.
[51] Z. Koudelkova, T. Syrovy, P. Ambrozova, Z. Moravec, L. Kubac, D. Hynek, L. Richtera, V. Adam, Determination of Zinc, Cadmium, Lead, Copper and Silver Using a Carbon Paste Electrode and a Screen Printed Electrode Modified with Chromium (III) Oxide, Sensors 17 (2017) 1832, https://doi.org/10.3390/s17081832.
[52] H. Farahani, R. Wagiran, M.N. Hamidon, Humidity Sensors Principle, Mechanism, and Fabrication Technologies: A Comprehensive Review, Sensors 14 (2014) 7881–7939.
[53] S.G. Ansari, Z.A. Ansari, R. Wahab, Y.S. Kim, G. Khang, H.S. Shin, Glucose sensor based on nano-baskets of tin oxide templated in porous alumina by plasma enhanced CVD, Biosens. Bioelectron. 23 (2008) 1838–1842.
[54] S.G. Ansari, R. Wahab, Z.A. Ansari, Y.S. Kim, G. Khang, A. Al-Hajry, H.S. Shin, Effect of nanostructure on the urea sensing properties of sol–gel synthesized ZnO, Sensors and Actuators B 137 (2009) 566–573.
[55] R.N. Mariammal, K. Ramachandran, Study on gas sensing mechanism in p-CuO/n-ZnO heterojunction sensor, Mater. Res. Bull 100 (2018) 420–428.